



**HAL**  
open science

## Large scale screening discovers clofoctol as an inhibitor of SARS-CoV-2 replication that reduces COVID-19-like pathology

Sandrine Belouzard, Arnaud Machelart, Valentin Sencio, Thibaut Vausselin, Eik Hoffmann, Nathalie Deboosere, Yves Rouillé, Lowiese Desmarets, Karin Séron, Adeline Danneels, et al.

### ► To cite this version:

Sandrine Belouzard, Arnaud Machelart, Valentin Sencio, Thibaut Vausselin, Eik Hoffmann, et al.. Large scale screening discovers clofoctol as an inhibitor of SARS-CoV-2 replication that reduces COVID-19-like pathology. 2021. hal-03357964

**HAL Id: hal-03357964**

**<https://hal.science/hal-03357964>**

Preprint submitted on 29 Sep 2021

**HAL** is a multi-disciplinary open access archive for the deposit and dissemination of scientific research documents, whether they are published or not. The documents may come from teaching and research institutions in France or abroad, or from public or private research centers.

L'archive ouverte pluridisciplinaire **HAL**, est destinée au dépôt et à la diffusion de documents scientifiques de niveau recherche, publiés ou non, émanant des établissements d'enseignement et de recherche français ou étrangers, des laboratoires publics ou privés.

# 1 Large scale screening discovers clofoctol as an inhibitor of SARS-CoV-2 2 replication that reduces COVID-19-like pathology 3

4 Sandrine Belouzard<sup>1</sup>, Arnaud Machelart<sup>1,6</sup>, Valentin Sencio<sup>1,6</sup>, Thibaut Vausselin<sup>1,2,6</sup>, Eik  
5 Hoffmann<sup>1</sup>, Nathalie Deboosere<sup>1,3</sup>, Yves Rouillé<sup>1</sup>, Lowiese Desmarets<sup>1</sup>, Karin Séron<sup>1</sup>, Adeline  
6 Danneels<sup>1</sup>, Cyril Robil<sup>1</sup>, Loïc Belloy<sup>2</sup>, Camille Moreau<sup>2</sup>, Catherine Piveteau<sup>4</sup>, Alexandre Biela<sup>4</sup>,  
7 Alexandre Vandeputte<sup>1,3</sup>, Séverine Heumel<sup>1</sup>, Lucie Deruyter<sup>1</sup>, Julie Dumont<sup>3,4</sup>, Florence  
8 Leroux<sup>3,4</sup>, Ilka Engelmann<sup>5</sup>, Enagnon Kazali Alidjinou<sup>5</sup>, Didier Hober<sup>5</sup>, Priscille Brodin<sup>1,3,7</sup>,  
9 Terence Beghyn<sup>2,7</sup>, François Trottein<sup>1,7</sup>, Benoît Déprez<sup>3,4,7\*</sup>, Jean Dubuisson<sup>1,7\*</sup>

10  
11  
12 <sup>1</sup>Univ Lille, CNRS, INSERM, CHU Lille, Institut Pasteur de Lille, U1019-UMR 9017-CIIL-Center  
13 for Infection and Immunity of Lille, Lille, France

14 <sup>2</sup>APTEEUS, Campus Pasteur Lille, 1 rue du Professeur Calmette, Lille, France

15 <sup>3</sup>Univ. Lille, CNRS, Inserm, CHU Lille, Institut Pasteur de Lille, US 41 - UMS 2014 - PLBS, F-  
16 59000 Lille, France

17 <sup>4</sup>Univ Lille, Inserm, Institut Pasteur de Lille, U1177-Drugs and Molecules for Living Systems,  
18 Lille, France

19 <sup>5</sup>Univ Lille, CHU Lille, Laboratoire de Virologie-ULR3610, Lille, France

20 <sup>6</sup>These authors contributed equally

21 <sup>7</sup>Equally contributing senior authors

22 \*corresponding authors: [jean.dubuisson@ibl.cnrs.fr](mailto:jean.dubuisson@ibl.cnrs.fr), [benoit.deprez@univ-lille.fr](mailto:benoit.deprez@univ-lille.fr)

## 23 **Abstract**

24 The fastest way to implement a treatment against a new rapidly emerging viral disease consists  
25 in screening the potential antiviral activity of drugs approved for human use. This has the  
26 advantage of shortening regulatory preclinical development steps. Here, we screened a library of  
27 drug compounds, already registered in one or several geographical areas, to identify those  
28 exhibiting antiviral activity against SARS-CoV-2 with relevant potency. Of the 1,942 compounds  
29 tested, 21 exhibited a substantial antiviral activity in Vero-81 cells. Among them, clofoctol, an  
30 antibacterial drug used for the treatment of bacterial respiratory tract infections, was further  
31 investigated due to its favorable safety profile and its pharmacokinetic properties. Notably, the  
32 peak concentration of clofoctol that can be achieved in human lungs is more than 20 times  
33 higher than its IC<sub>95</sub> measured against SARS-CoV-2 in human pulmonary cells. Mechanistically,  
34 this compound inhibits SARS-CoV-2 at a post-entry step by specifically blocking translation  
35 initiation of viral RNA. Lastly, therapeutic treatment of human ACE2 receptor transgenic mice  
36 decreased viral load, reduced inflammatory gene expression and improved pulmonary  
37 pathology. Altogether, these data strongly support clofoctol as a therapeutic candidate for the  
38 treatment of COVID-19 patients.

1  
2 The coronavirus disease 2019 (COVID-19) is having a catastrophic impact on human health as  
3 well as on the global economy, and it will continue to affect our lives for years to come<sup>1</sup>. This  
4 pandemic requires the urgent development of specific therapeutics and vaccines. While several  
5 vaccines are now licensed, we still lack affordable efficient therapies against SARS-CoV-2.  
6 Antivirals are urgently needed to treat COVID-19 patients who have not yet been vaccinated and  
7 as a therapeutic approach to treat vaccinated people unprotected against SARS-CoV-2 variants.  
8 Repurposing clinically evaluated drugs can potentially offer a fast track for the rapid deployment  
9 of treatments for this kind of emerging infectious disease. However, the first attempts of targeted  
10 repurposing strategies to treat COVID-19 patients have led to disappointing results<sup>2</sup>. As an  
11 alternative approach, large-scale screening of clinically approved drugs through a carefully  
12 designed evaluation cascade may identify additional unanticipated therapeutic options that can  
13 be positioned for accelerated clinical evaluation<sup>3-5</sup>. Here, we developed a high-content screen  
14 (HCS) using the Apteeus drug library (TEELibrary®), a comprehensive collection of 1,942  
15 approved drugs, to identify molecules that exhibit antiviral activity against SARS-CoV-2.  
16 Clofoctol was selected based on its antiviral potency associated with favorable pharmacokinetic  
17 properties in human. Its further validation in a small-animal model makes it a promising  
18 candidate treatment for clinical evaluation in COVID-19 patients.

## 19 **HCS screening of a library of approved drugs**

20 The screen was performed in Vero-81 cells, an African green monkey kidney cell line highly  
21 permissive to SARS-CoV-2 infection<sup>6</sup>. The read out was based on the cytopathic effect (CPE) of  
22 the virus as measured by propidium iodide (PI) incorporation into the nuclei of dying cells and  
23 cell quantification by nuclei staining with Hoechst 33342 (Supplementary Fig. 1a, Supplementary  
24 Table 1). Assay parameters, including cell seeding density, multiplicity of infection (MOI) and  
25 time points, were optimized in Vero-81 cells by measuring virus-induced CPE in a 384-well  
26 format.

27 To assess reproducibility of the optimized assay in a HCS configuration, we initially evaluated  
28 the effect of chloroquine (CQ), previously reported to have antiviral activity against SARS-CoV-2  
29 in Vero Cells<sup>7</sup>. This enabled us to benchmark the dynamic range of the assay with a reliable  
30 positive control. Robustness was then assessed by calculating the strictly standardized mean  
31 difference (SSMD) of each plate, with a mean of 6.87 ( $\pm 2.19$ ) for all plates (Supplementary Fig.  
32 1b). We then used this experimental design to screen our drug library (Fig. 1a) using a non-  
33 cytotoxicity concentration of 15  $\mu$ M for most compounds in the presence of low viral input (MOI =  
34 0.01), in order to capture multicycle replication with an extended end-point measurement at 72h  
35 post-infection<sup>4</sup>. For each compound, a Robust Z-score normalized to the median of each plate

1 was calculated for both SARS-CoV-2-induced CPE related readouts (PI measurement and  
2 Hoechst 33342 staining).

3 Compounds exhibiting the highest levels of CPE inhibition were initially selected. Of the 1,942  
4 tested compounds, 57 were identified to significantly decrease PI incorporation (robust Z-core <  
5 -3) or increase the number of cells as measured with Hoechst 33342 staining (robust Z-score >  
6 3) (Supplementary Table 2). Among these compounds, CQ, nitazoxanide, amodiaquine,  
7 triflupromazine and niclosamide were previously identified in other studies<sup>3,7-9</sup> (Fig. 1**b**). It is  
8 worth noting that the majority of the selected compounds are basic molecules like CQ,  
9 amodiaquine, fluphenazine, trifluoperazine and triflupromazine (Fig. 1**c**). Such compounds are  
10 known to affect the endosomal internalization pathway by accumulating inside the endosomes,  
11 modifying their pH and therefore inhibiting SARS-CoV-2 by blocking its endosomal entry.

12 We assessed the activity of the 57 identified hits in dose-response curve (DRC) analyses using  
13 the same setting as in the screen (Supplementary Table 2). Of these, 21 showed dose-related  
14 inhibition of the PI incorporation upon infection (N=2).

15 Coronaviruses, including SARS-CoV-2, can use two different routes to enter their target cells.  
16 They either enter cells by endocytosis and release their genome into the cytosol after fusion of  
17 their envelope with an endosomal membrane, or they fuse their envelope directly with the  
18 plasma membrane. This latter entry route is triggered by the cell surface protease TMPRSS2  
19 which is not expressed in Vero-81 cells<sup>10</sup>. Previously identified anti-SARS-CoV-2 compounds,  
20 like CQ and hydroxy-CQ, were shown to only block the endocytic entry route<sup>10</sup>. As expected, CQ  
21 did not exhibit an antiviral activity in the context of Vero-81 cells ectopically expressing  
22 TMPRSS2 (Vero-81-TMPRSS2)(Fig. 1 **d** and **e**). Notably, hydroxy-CQ produced no measurable  
23 positive outcomes in clinical trials<sup>2</sup>. An additional validation on Vero-81-TMPRSS2 cells was  
24 therefore performed to discard compounds that only block the endocytic route of SARS-CoV-2  
25 entry.

26 Of the 21 molecules validated twice in Vero-81 cells, the most interesting ones were retained  
27 based on a preliminary evaluation of their risk/benefit ratio in the clinic. This evaluation included  
28 a comparison of the *in vitro* potency to plasma exposure at the approved dose. Therefore, 8 out  
29 of the 21 compounds were tested in Vero-81-TMPRSS2 cells (Supplementary Table 2). Only 3  
30 of them exhibited a dose-dependent antiviral activity against SARS-CoV-2 in the presence or  
31 absence of TMPRSS2, indicating an antiviral effect irrespective of the entry route, among which  
32 perphenazine, nitazoxanide, and one, called clofoctol, that was not reported by others (Fig. 1 **d**  
33 and **e**). In Vero-81 cells, the IC<sub>50</sub> and IC<sub>95</sub> of this latter compound were 4µM and  
34 10µM, respectively, and its potency was maintained in TMPRSS2-expressing cells. More  
35 importantly, clofoctol is well distributed in tissues, particularly in lungs where its concentration is

1 twice higher than in plasma<sup>11</sup>. Altogether, these observations prompted us to further characterize  
2 the anti-SARS-CoV-2 properties of clofoctol.

### 3 ***In vitro* validation of the antiviral activity of clofoctol**

4 To further confirm the antiviral activity of clofoctol, SARS-CoV-2 genomic replication was  
5 measured by quantitative RT-PCR. In this assay, clofoctol exhibited an IC<sub>50</sub> and an IC<sub>95</sub> of 4 μM  
6 and 12 μM, respectively (Fig. 2a). To validate the specificity of its antiviral activity, its potential  
7 cytotoxic effect in cell culture was determined in an MTS viability assay. As shown in Fig. 2b,  
8 after 24h of treatment, no cytotoxic effect was observed at concentrations below 40 μM,  
9 indicating that the decreased SARS-CoV-2 replication in the presence of clofoctol was not due to  
10 a cytotoxic effect of the compound. To further characterize the antiviral activity of clofoctol, its  
11 effect on the production of infectious progeny virions was also quantified. As shown in Fig. 2c, a  
12 dose-dependent decrease of infectious virus production was observed in these experimental  
13 conditions, confirming the antiviral effect of clofoctol against SARS-CoV-2.

14 Vero cells are the cells of choice to efficiently grow SARS-CoV-2 in culture and therefore to  
15 screen large libraries of compounds for rapid identification of antivirals. However, as these cells  
16 are from monkey origin, the human cell line Calu-3, derived from a lung adenocarcinoma,  
17 previously shown to be permissive to SARS-CoV-2<sup>10</sup> was also used to validate our  
18 observations. As shown in Fig. 2d, a dose-dependent decrease of viral RNA production was also  
19 observed in infected Calu-3 cells treated with clofoctol, at concentrations that did not exhibit a  
20 cytotoxic effect (Fig. 2b).

### 21 **Clofoctol inhibits the translation of SARS-CoV-2 viral RNAs**

22 The life cycle of a virus can be divided into three major steps: (1) entry, (2) translation/replication  
23 and (3) assembly/release. To determine at which step clofoctol inhibits SARS-CoV-2, the  
24 compound was added either before infection, during virus entry, post-inoculation or throughout  
25 all the steps. Remdesivir, an inhibitor of the viral polymerase<sup>12</sup>, and CQ were used as control  
26 antivirals affecting viral replication or entry, respectively. As shown in Fig. 3a, clofoctol inhibited  
27 SARS-CoV-2 mainly at the post-inoculation step. This was similar to the inhibitory profile  
28 observed with remdesivir, although clofoctol also had a mild effect at the entry step. These data  
29 suggest that the translation/replication step is likely the major target of clofoctol. To further  
30 characterize the post-entry inhibitory effect of clofoctol, a time-of-addition experiment was also  
31 performed in parallel with clofoctol, remdesivir and CQ. In this experiment, the compounds were  
32 added before infection or at different times post-infection. As shown in Fig. 3b, the inhibitory  
33 effects of clofoctol and remdesivir were very similar, whereas CQ showed a very different profile.  
34 Thus, this latter compound was only efficient when added prior to infection or during the  
35 inoculation step, whereas remdesivir and clofoctol were also effective when added up to three

1 hours post-inoculation. To further investigate a potential effect of clofoctol on SARS-CoV-2 entry,  
2 we used retroviral particles pseudotyped with the SARS-CoV-2 Spike (S) glycoprotein  
3 (SARS2pp). These are retroviral cores carrying SARS-CoV-2 S glycoproteins in their envelope.  
4 In this context, only the early steps of the viral life cycle (i.e., virus interaction with receptors,  
5 uptake, and fusion) are SARS-CoV-2 specific, whereas all later steps are dependent on  
6 retroviral nucleocapsid elements. Clofoctol did not show any inhibitory effect on SARS2pp entry  
7 (Fig. 3c), indicating that it does not inhibit the cellular entry of SARS-CoV-2. Of note, clofoctol  
8 was also active against another coronavirus which is mildly pathogenic, HCoV-229E, and more  
9 importantly against the B.1.1.7 and the D614G variants of SARS-CoV-2 (Supplementary Fig. 2),  
10 indicating that its antiviral activity is conserved across different clades of SARS-CoV-2 and  
11 coronavirus species.

12 For positive-stranded RNA viruses like coronaviruses, translation of the viral genome is the step  
13 that immediately follows virus entry. To determine whether this step is affected by clofoctol  
14 treatment, we used a reporter construct expressing the *Renilla* luciferase introduced between  
15 the 5'-UTR and the 3'-UTR of the SARS-CoV-2 genomic RNA. As a control, we used a  
16 bicistronic construct containing the *Firefly* luciferase sequence under the control of a eukaryotic  
17 mRNA 5' cap structure, followed by the *Renilla* luciferase sequence under the translational  
18 control of the hepatitis C virus (HCV) IRES<sup>13</sup>. To avoid a potential effect of clofoctol on the  
19 transcription of the reporters from plasmid DNA, *in vitro*-transcribed capped RNAs were  
20 transfected by electroporation into Vero-81 or Huh-7 cells. After 8h of clofoctol treatment, a  
21 dose-dependent inhibition of luciferase activity was observed with the SARS-CoV-2 UTRs-based  
22 construct in Vero-81 and Huh-7 cells, but not for the control bicistronic construct (Fig. 3d),  
23 indicating that clofoctol specifically inhibits the translation of an mRNA containing the UTRs of  
24 the SARS-CoV-2. This suggests that clofoctol has the potential to inhibit the translation of  
25 genomic as well as sub-genomic SARS-CoV-2 RNAs.

## 26 **Clofoctol inhibits SARS-CoV-2 replication *in vivo* and lowers inflammation in lungs**

27 To investigate the potential antiviral activity of clofoctol against SARS-CoV-2 *in vivo*, we took  
28 advantage of transgenic C57BL/6 mice expressing the human ACE2 receptor (K18-hACE2  
29 mice)<sup>14</sup>. Before testing the potential antiviral activity of clofoctol, pharmacokinetic experiments  
30 were performed in female C57BL/6 mice. To this end, clofoctol was injected intraperitoneally  
31 (i.p.) at 62.5 mg/kg to reach a lung concentration close to that achieved in humans at approved  
32 posology. Mice were sacrificed at 30 min, 1h, 2h and 4h after i.p. administration of clofoctol. As  
33 early as 30 min after injection, clofoctol reached concentrations up to 61  $\mu$ M in the lungs and  
34 remained above this level for almost 4h (Fig. 4a, *left panel*), whereas it remained at a  
35 concentration seven times lower in the plasma. According to its expected half-life in the lungs,

1 clofoctol concentration was anticipated to remain above its *in vitro* measured IC<sub>95</sub> (IC<sub>95</sub> ~10μM)  
2 for more than 7 consecutive hours. It was then decided to treat the mice twice daily to maintain a  
3 lung concentration close to 60 μM. In this setting, clofoctol concentration reached 67 μM in the  
4 lungs, 1h after the fourth administration (Fig. 4a, *right panel*).

5 Because of this favorable pharmacokinetic profile in mice, we decided to test clofoctol in K18-  
6 hACE2 transgenic mice. Female mice were inoculated intranasally (i.n.) with 5x10<sup>2</sup> TCID<sub>50</sub> of a  
7 clinical SARS-CoV-2 isolate. The animals were then injected intraperitoneally with clofoctol at 1h  
8 and 8h post-infection. This treatment was repeated the day after infection and some of the mice  
9 were sacrificed at day 2 post-inoculation (Fig. 4b, *upper panel*). As compared to untreated  
10 animals, the infectious viral load detected in the lungs of clofoctol-treated mice was reduced by  
11 more than 1.1 log<sub>10</sub> at day 2 post-infection (Fig. 4b, *left panel*). Analysis of viral RNA yields by  
12 RT-qPCR confirmed the reduced viral load in clofoctol-treated animals (Fig. 4b, *right panel*).  
13 Male K18-hACE2 transgenic mice are more susceptible than females to SARS-CoV-2  
14 infection<sup>14</sup>. Clofoctol treatment similarly reduced the viral load in the lungs of male K18-hACE2  
15 transgenic mice (Supplementary Fig. 3a).

16 We then investigated whether the decrease in viral load would have positive effects on lung  
17 inflammation. Remarkably, the expression of transcripts encoding IL-6, TNFα, IL12p40, IFNβ,  
18 IFNγ and the interferon-stimulated genes (ISG) Mx1, Ifi44 and ISG15 was markedly reduced in  
19 clofoctol-treated mice, in contrast with that of IL-17A (Fig. 4c, *upper panel*). Similar results were  
20 also observed in male K18-hACE2 transgenic mice (Supplementary Fig. 3b). At day 4 post-  
21 inoculation, mice treated during the first 2 days with clofoctol still showed a decrease in viral load  
22 (Supplementary Fig. 4a). Expression of transcripts encoding inflammatory markers was also  
23 strongly decreased at day 4 post-infection (supplementary Fig. 4b and data not shown). At this  
24 time point, SARS-CoV-2 infection was associated with reduced expression of genes encoding  
25 markers of epithelial barrier function, including the tight-junction protein Zonula Occludens-1  
26 (ZO-1) and occludin. Interestingly, the drop of these transcript levels induced by SARS-CoV-2  
27 infection was significantly reduced in clofoctol-treated animals (supplementary Fig. 4c).

28 Lastly, we assessed the impact of clofoctol treatment on lung pathology at day 4 post-infection.  
29 In vehicle-treated animals, a mild multifocal broncho-interstitial pneumonia was observed (Fig.  
30 4d, *upper right panel*). Signs of moderate inflammation (red square), with the presence of  
31 neutrophils, macrophages and a few lymphocytes, were observed within alveolar lumens, inter-  
32 alveolar septa, and perivascular spaces which was accompanied by minimal perivascular edema  
33 (red arrows) (Fig. 4d, *lower right panel*). Slight vascular congestion and discrete intra-alveolar  
34 hemorrhages were also detected (not shown). In stark contrast, only a minimal interstitial  
35 inflammation was observed in clofoctol-treated mice (Fig. 4d, *upper left panel*), with a limited  
36 presence of macrophages and lymphocytes within inter-alveolar septa and little vascular

1 congestion (Fig. 4d, lower left panel). We conclude that, at doses that produce lung  
2 concentrations close to those observed in human patients treated at the approved dose,  
3 clofoctol treatment in mice just after infection lowers SARS-CoV-2 replication and reduces lung  
4 pathological features associated with this viral infection.

## 5 **Discussion**

6 In this study, we report the high-throughput screening of ~2,000 drugs, approved for human use,  
7 for their potential activity against SARS-CoV-2. Our data identify clofoctol as a promising  
8 antiviral candidate for the treatment COVID-19 patients. This antibacterial drug was developed in  
9 the late 1970s. Its efficacy has been demonstrated for the treatment of *Streptococcus*  
10 *pneumoniae* - the leading cause of bacterial pneumonia worldwide - and *Staphylococcus aureus*  
11 <sup>15,16</sup>. The drug was marketed in France until 2005 under the trade name Octofène® and is still  
12 prescribed in Italy under the trademark GramPlus®. Mechanistically, clofoctol inhibits bacterial  
13 cell wall synthesis and induces membrane permeabilization<sup>17,18</sup>. Along with its bactericidal  
14 activity, clofoctol was recently shown to also inhibit protein translation and to impair tumor cell  
15 growth<sup>19,20</sup>. As such, clofoctol could be useful to treat some cancers and possibly other  
16 diseases<sup>21</sup>.

17 Among the 2,000 drugs tested, clofoctol emerged as the most promising compound to inhibit  
18 SARS-CoV-2 replication in our experimental settings. Mechanistically, it inhibits SARS-CoV-2  
19 propagation by blocking translation of viral RNA. This inhibition could be due to the activation of  
20 the unfolded protein response (UPR) pathways. Clofoctol has indeed been reported to induce  
21 endoplasmic reticulum (ER) stress and to activate all three UPR pathways, i.e. the inositol  
22 requiring enzyme 1 (IRE1), the double stranded RNA-activated PK-like ER kinase (PERK), and  
23 the activating transcription factor 6 (ATF6)<sup>22</sup>. Modulation of UPR pathways was previously  
24 reported to inhibit the replication of viruses including coronaviruses. Thus, modulating the PERK-  
25 eIF2 $\alpha$  pathway can inhibit the replication of the transmissible gastroenteritis porcine  
26 coronavirus<sup>23</sup>. Similarly, triggering the UPR with 2-deoxy-D-glucose inhibits the replication of  
27 another coronavirus, the porcine epidemic diarrhea virus<sup>22</sup>. Whether the clofoctol-induced  
28 inhibition of SARS-CoV-2 translation is linked to UPR activation will be the focus of further  
29 investigation.

30 Previous pharmacokinetic studies indicate that clofoctol is well absorbed by rectal  
31 administration, and can rapidly expose lung tissues<sup>11,24</sup>. Of interest, as early as 90 minutes after  
32 rectal administration, the peak concentration of clofoctol that can be achieved in human lungs is  
33 more than 20 times higher than its IC<sub>95</sub> measured in Vero-81 cells. In our experimental  
34 conditions, clofoctol was also detected in mice lungs at a peak concentration reaching  
35 approximately tenfold its IC<sub>95</sub>. Notably, upon two days of treatment with doses allometrically



1 similar to those approved for human treatment, its concentration remained far above the IC<sub>95</sub> in  
2 the lungs. Importantly, we demonstrate here that clofoctol treatment decreased the viral load in  
3 the lungs and drastically reduced pulmonary inflammation. These *in vivo* data, as well as the  
4 rapid onset of action expected in human pharmacokinetics, strongly support clofoctol as a  
5 therapeutic candidate for the treatment of COVID-19 patients. A phase 2/3 placebo controlled  
6 clinical trial is planned to further validate the therapeutic potential of this compound in the early  
7 phase of COVID-19.

8 Together with its antiviral effects, clofoctol abrogated lung inflammation. To the best of our  
9 knowledge, the anti-inflammatory effect of clofoctol has never been reported before. Together  
10 with its effect on UPR pathways, clofoctol is known to interact with different targets including (i)  
11 the Cdc7/Dbf4 protein kinase complex, which regulates the initiation of DNA replication and (ii)  
12 the upstream-of-N-Ras protein (UNR), a highly conserved RNA-binding protein known to  
13 regulate gene expression. Of interest, by binding to UNR, clofoctol activates the transcription  
14 factor Kruppel-like factor 13 (KLF13)<sup>20</sup>, known as a tumor suppressor gene and as a regulator of  
15 T cell differentiation<sup>25,26</sup>. Whether the UNR/KMF13 pathway triggered by clofoctol plays a role in  
16 decreasing inflammation during SARS-CoV-2 infection deserves further investigation. Additional  
17 functional studies are urgently needed to assess the global effect of clofoctol on COVID-19  
18 pathology.

19 In conclusion, the antiviral and anti-inflammatory properties of clofoctol, associated with its  
20 safety profile and unique pharmacokinetics make a strong case for proposing clofoctol as an  
21 affordable therapeutic candidate for the treatment of COVID-19 patients.

22

## 23 **Methods**

24 **Data reporting.** No statistical methods were used to predetermine sample size. Compounds  
25 were spotted in a randomized order on the plates during the primary screen. All the other  
26 experiments were not randomized. Investigators were blinded to allocation during the primary  
27 screen and the corresponding validation, during both assay performance and outcome  
28 assessment. For all the other assays, the investigators were not blinded.

29

30 **Cells and viruses.** Vero-81 cells (ATCC, CCL-81), Vero-E6 cells (ATCC, CRL-1586), Huh-7  
31 cells<sup>27</sup> and HEK293T/17 cells (ATCC, CRL-11268) were grown at 37°C with 5% CO<sub>2</sub> in  
32 Dulbecco's modified eagle medium (DMEM, Gibco) supplemented with 10 % heat-inactivated  
33 fetal bovine serum (FBS, Eurobio). Calu-3 cells (Clinisciences, EP-CL-0054) were grown in  
34 minimum essential medium (Gibco, MEM) supplemented with glutamax (Gibco) and 10% heat-  
35 inactivated FBS.

1 Lentiviral vectors expressing TMPRSS2 were produced by transfection of HEK293T cells with  
2 pTRIP-TMPRSS2, pHCMV-VSVG and HIV gag-pol in the presence of Turbofect (Life  
3 Technologies) according to the manufacturer's instruction. Supernatants were collected at 48h  
4 post-transfection and used to transduce Vero-E6 cells.  
5 The BetaCoV/France/IDF0372/2020 strain of SARS-CoV-2 was supplied by the French National  
6 Reference Center for Respiratory Viruses hosted by Institut Pasteur (Paris, France). The hCoV-  
7 19\_IPL\_France strain of SARS-CoV-2 (NCBI MW575140) was also used in some experiments.  
8 The virus was propagated in Vero-E6 cells expressing TMPRSS2 by inoculation at MOI 0.01.  
9 Cell supernatant medium was harvested at 72h post-infection and stored frozen at -80 °C in  
10 small aliquots ( $2 \times 10^6$  TCID<sub>50</sub>/mL). All experiments were conducted in a BSL3 laboratory.

11 **Chemical libraries.** The TEELibrary®, built and supplied by APTEEUS company, is a collection  
12 of 1,942 bioactive compounds. This library contains approved drugs for human use (FDA, EMA  
13 and other agencies). The compounds are provided at a non-cytotoxic concentration, the majority  
14 of them are prepared at a 10mM concentration in compatible solvent (DMSO for the majority of  
15 them). CQ diphosphate was purchased from Sigma-Aldrich (Dorset, England and St. Louis,  
16 MO). CQ diphosphate was diluted to a final concentration of 10 mM in water. Clofoctol  
17 was purchased from Sigma-Aldrich (C2290) or provided by Chiesi company.

18 **Drug screening assay.** One day prior to infection, Vero-81 cells were seeded in black 384-well  
19 µClear® plates (Greiner Bio-One), at a density of 3,000 cells per well in 30 µl DMEM,  
20 supplemented with 10% FBS and 1X Penicillin-Streptomycin solution (Gibco), using MultiDrop  
21 Combi® Reagent dispenser (ThermoFischer Scientific). The next day, compounds from the  
22 TEELibrary® were first dispensed into the 384-well plates, using an Echo 550 Liquid Handler  
23 (Labcyte). To identify the compounds of interest, they were tested at a final compound  
24 concentration that usually does not induce cytotoxicity, most of them at 15 µM. On each plate,  
25 five 3-fold serial dilutions of CQ diphosphate ranging from 0.15 µM to 15 µM were added in six  
26 replicates, as a control compound of viral inhibition (positive controls). Eleven control virus wells  
27 devoid of compound and scattered over the plate, were supplemented with 0.15% DMSO or  
28 0.15% H<sub>2</sub>O (negative controls), respectively. Cells were infected by adding 10 µL of SARS-CoV-  
29 2 per well at a MOI of 0.01 in 10% FBS-containing medium, using a Viafill Rapid Reagent  
30 Dispenser (Integra). The plates were then incubated at 37° with 5% CO<sub>2</sub>. At 3 days post-  
31 infection, cells were stained with 10 µg/mL Hoechst 33342 dye (Sigma-Aldrich) and 1 µg/mL PI  
32 (ThermoFischer Scientific) for 30 min at 37°C for CPE quantification by high-content imaging.

33 **Dose response curves, EC<sub>50</sub> calculations and hit validations.** The selected hits were further  
34 validated in a 6-point dose-response confirmation assay for EC<sub>50</sub> determination. One day prior to  
35 infection, Vero-81 cells were seeded in 384-well plates, as previously described. The next day,

1 six 3-fold serial dilutions of compounds (0.15 to 45  $\mu\text{M}$ , in duplicate) were first added to the cells.  
2 Ten  $\mu\text{L}$  of virus diluted in medium was then added to the wells. On each plate, twenty-six virus  
3 control wells distributed over the plates were supplemented with 0.15% DMSO and  $\text{H}_2\text{O}$ ,  
4 respectively. CQ diphosphate was added as a control compound, at six 3-fold serial dilutions  
5 (0.15  $\mu\text{M}$  to 45  $\mu\text{M}$ , in duplicate). Plates were incubated for 3 days at 37°C prior to staining and  
6 CPE quantification by high-content imaging.

7 **Image acquisition.** Image acquisitions were performed on a high-resolution automated confocal  
8 microscope (Opera, PerkinElmer) using a 10x air objective for cellular infection assay. Hoechst  
9 33342-stained nuclei were detected using the 405 nm excitation laser (Ex) with a 450/50-nm  
10 emission filter (Em). Red signal, corresponding to PI-stained nuclei from dead cells, was  
11 detected using Ex at 561 nm and Em at 600 nm. A set of 3 fields was collected from each well.

12 **Image-based analysis.** For total cell and dead cell detection, images from the automated  
13 confocal microscope were analyzed using multi-parameter scripts developed using Columbus  
14 system (version 2.3.1; PerkinElmer) (Supplementary Table 1). A segmentation algorithm was  
15 applied to detect nuclei labeled by Hoechst 33342 (blue) and determine total nuclei number.  
16 Briefly, a mask was first determined from input image, using the intensity threshold of Hoechst  
17 dye signal to create a region of interest corresponding to Hoechst-stained population. The nuclei  
18 segmentation was then performed using the algorithm "Find Nuclei", as described previously<sup>28</sup>.  
19 Morphology properties, as area and roundness, could be used to exclude smaller objects not  
20 corresponding to nuclei. The total number of cells was quantified as Hoechst-positive nuclei.  
21 Red fluorescence signal intensities in the previous selected nuclei were quantified and used for  
22 the selection of PI positive (PI+) and negative (PI-) nuclei. Subsequently, population of dead  
23 (PI+) and viable (PI-) cells were determined. The percentage of PI+ cells was calculated for each  
24 compound to select drugs having an effect on the decrease of cell death, corresponding to  
25 infection or viral replication inhibition.

26 **Dose-response validation in different cell lines.** Vero-81, Vero-81-TMPRSS2 or Calu-3 cells  
27 were infected in duplicates at a MOI of 0.25 in the presence of increasing concentrations of  
28 clofoctol, ranging from 0 to 25  $\mu\text{M}$ , and incubated either for 6h (Vero-81 cells) or 24h (Calu-3  
29 cells). Then total RNA was extracted by using the Nucleospin RNA kit (Macherey Nagel) as  
30 recommended by the manufacturer. Genome quantification was performed as described<sup>29</sup>.

31 **Viral secretion.** Vero-81 and Vero-81-TMPRSS2 cells were infected at a MOI of 0.25 for 1h,  
32 then the cells were rinsed 3 times with PBS and further incubated in the presence of increasing  
33 concentrations of clofoctol for 16h. Each condition was performed in duplicates. Cell  
34 supernatants were collected and viral titer were measured by the TCID<sub>50</sub> method.

1 **Pseudoparticles infection.** Retroviral Murine leukemia virus particle were pseudotyped with the  
2 SARS-CoV-2 Spike (BetaCoV/France/IDF0372/2020 strain) or the glycoprotein of the vesicular  
3 stomatitis virus (VSV-G). Briefly, HEK293T cells were co-transfected with a plasmid encoding  
4 Gag-Pol (pTG-Gag-Pol), a plasmid encoding the envelope glycoprotein and a plasmid containing  
5 a minigenome with a *Firefly* luciferase reporter gene. After 48h of incubation, cell supernatants  
6 were collected, filtered and used to transduce Huh-7 cells expressing human ACE2 in the  
7 presence of increasing concentrations of clofoctol or CQ. Transduced cells were lysed 48h later  
8 and luciferase activity was measured by using the luciferase assay system (Promega).

9 **Time-of-addition experiment.** Vero-81 cells were plated in 24-well plates and infected for 1h at  
10 a MOI of 0.5. Clofoctol, remdesivir or CQ were added to the cells at a concentration of 15  $\mu$ M  
11 every hour starting one hour before inoculation. At 8h post-infection, the cells were lysed in non-  
12 reducing Laemmli loading buffer. Proteins were separated onto a 10% SDS-polyacrylamide gel  
13 electrophoresis and transferred on nitrocellulose membranes (Amersham). Membrane-bound N  
14 proteins were detected with a rabbit polyclonal antibody (Novus) and a horseradish peroxidase-  
15 conjugated secondary antibody (Jackson Immunoresearch). Detection was carried out by  
16 chemoluminescence (Pierce) and signals were quantified by using the gel quantification function  
17 of ImageJ. The experiment was repeated 3 times in duplicates.

18 **Immunofluorescence.** Vero-81 cells were plated onto glass coverslips. The day after, the cells  
19 were infected for 1h with SARS-CoV-2 at a MOI of 0.25. Clofoctol, remdesivir or CQ were added  
20 at 15  $\mu$ M at different steps of the infection. The cells were either incubated 1h before inoculation  
21 (pre-incubation) or during the inoculation and for 1h after virus removal (entry step) or starting 1h  
22 after the inoculation until cell fixation (post-entry). Additional conditions with the compounds  
23 present during the whole experiment were also included as well as controls with DMSO or H<sub>2</sub>O.  
24 Cells were incubated for 16h after infection and fixed with 4% paraformaldehyde. Then, cells  
25 were permeabilized for 5 min with 0.1% Triton X-100 in PBS and blocked for 30 min with 5%  
26 goat serum in PBS. Infected cells were detected by using an anti-dsRNA (J2 monoclonal  
27 antibody, Scicons) diluted in blocking buffer to detect the presence of replicating SARS-CoV-2  
28 virus as previously determined<sup>29</sup>. After a 30-min incubation, cells were rinsed 3 times for 5 min in  
29 PBS and incubated for 30 min with a cyanine 3-conjugated goat anti-mouse secondary antibody  
30 (Jackson Immunoresearch) and DAPI (4',6-diamidino-2-phenylindole).

31 The coverslips were rinsed with PBS 3 times for 5 min followed by a final water wash before  
32 mounting on microscope slides in Mowiol 4-88 containing medium. Images acquisitions were  
33 performed with an EVOS M5000 imaging system (Thermo Fischer Scientific) equipped with a  
34 10X objective and light cubes for DAPI and RFP. The total number of cells was determined by  
35 counting the number of nuclei and the number of infected cells was determined by counting  
36 dsRNA-positive cells. The experiment was performed three times.

1 **Viability assay.** Vero cells, Huh-7 cells or Calu-3 cells were plated in 96-well plates and were  
2 then incubated the next day in 100 µl of culture medium containing increasing concentrations of  
3 clofoctol for 24h. An MTS [3-(4,5-dimethylthiazol-2-yl)-5-(3-carboxymethoxyphenyl)-2-(4-  
4 sulfophenyl)-2H-tetrazolium]-based viability assay (CellTiter 96 aqueous nonradioactive cell  
5 proliferation assay, Promega) was performed as recommended by the manufacturer. The  
6 absorbance of formazan at 490 nm is detected using an enzyme-linked immunosorbent assay  
7 (ELISA) plate reader (ELx808, BioTek Instruments, Inc.). Each measure was performed in  
8 triplicate.

9 **Analysis of the effect of the drug on translation.** A plasmid containing a synthetic gene  
10 encompassing the 5'-UTR (nucleotides 1-265) and the 3'UTR (nucleotides 29675-29903) of  
11 SARS-CoV-2 isolate Wuhan-Hu-1 (Genebank NC\_045512.2) separated by two head-to-tail BbsI  
12 sites was produced by GeneCust. The coding sequence of *Renilla* luciferase amplified by PCR  
13 using primers containing BbsI sites was inserted between both UTRs by ligation of BbsI-  
14 restricted PCR and plasmid. In this way, the coding sequence of the luciferase was inserted  
15 between the UTRs without leaving an extra nucleotide in between. The plasmid was linearized  
16 by NsiI restriction, and the linearized DNA was then used as a template for *in vitro* transcription  
17 with the mMMESSAGE mMACHINE T7 kit from Thermofischer Scientific, as recommended by the  
18 manufacturer. *In vitro*-transcribed capped RNA was delivered to Vero-81 and Huh-7 cells by  
19 electroporation. Cells were cultured for 8h in the presence of increasing concentrations of  
20 clofoctol. *Renilla* luciferase activities were measured with a *Renilla* luciferase assay from  
21 Promega. As a control, we used a bicistronic construct containing the *Firefly* luciferase sequence  
22 under the control of a cap structure, followed by the *Renilla* luciferase under the control of  
23 hepatitis C virus (HCV) IRES. *Firefly* and *Renilla* luciferase activities were measured with a dual-  
24 luciferase reporter assay system from Merck Millipore as previously reported<sup>13</sup>.

#### 25 **Pharmacokinetic study.**

26 Clofoctol diluted in 1.75% final Kolliphor® RH40 (07076, Sigma) and 1.4% final ethanol in a  
27 sodium chloride solution (0.9%) was used for intraperitoneal (i.p.) injection (62.5 mg/kg in  
28 females and 50 mg/kg in male). The concentration of clofoctol in plasma and lungs was  
29 measured at different time points post-clofoctol inoculation. Plasma samples and lung tissues  
30 were collected and treated with absolute ethanol, in a ratio of 1 to 10 and 1 to 50, respectively.  
31 Lung tissues were homogenized with a mechanical lysis system (Tissue Lyzer II). Supernatants  
32 were obtained by centrifugation before injection in LC-MS/MS. Samples were analysed using  
33 UPLC system Acquity I Class (Waters), combined with a triple quadrupole mass spectrometer  
34 Xevo TQD (Waters). The column, placed at 40°C, was an Acquity BEH C8 50\*2.1mm, 1.7µm  
35 column (Waters) and the following mobile phases were used: 5mM ammonium formate pH 3.75  
36 in water, as solvent (A) and 5 mM ammonium formate pH 3,75 in acetonitrile as solvent.

## 1 **Experimental infection of K18-hACE2 transgenic mice**

2 Eight week-old K18-human ACE2 expressing C57BL/6 mice (B6.Cg-Tg(K18-hACE2)2PrImn/J)  
3 were purchased from the Jackson Laboratory. For infection, mice (both sexes) were  
4 anesthetized by i.p. injection of ketamine (100 mg/kg) and xylazine (10 mg/kg) and then  
5 intranasally infected with 50  $\mu$ l of DMEM containing (or not, in a mock sample)  $5 \times 10^2$  TCID<sub>50</sub> of  
6 hCoV-19\_IPL\_France strain of SARS-CoV-2 (NCBI MW575140). Clofocetol (62.5 mg/kg in  
7 females and 50 mg/kg in males) was injected i.p. at 1h and 8h post-infection. The treatment was  
8 repeated the day after infection. Mice were sacrificed at day 2 or day 4 post-infection.

## 9 10 **Determination of viral loads in the lungs of mice**

11 To determine the viral loads in lungs, half of right lobes were homogenized in Lysing Matrix D  
12 tubes (mpbio) containing 1 mL of PBS using Mixer Mill MM 400 (Retsch) (15min – 15 Hz). After  
13 centrifugation at 11,000 rpm for 5 min, the clarified supernatant was harvested for virus  
14 titration. Dilutions of the supernatant were done in DMEM with 1% penicillin/streptomycin and  
15 dilutions were transferred to Vero-E6 cells in 96-well plates for TCID<sub>50</sub> assay. Quantitation of  
16 viral RNA in lung tissue was performed as follows. Briefly, half of the left lobe was homogenized  
17 in 1mL of RA1 buffer from the NucleoSpin RNA kit containing 20 mM of Tris(2-  
18 carboxyethyl)phosphine). Total RNAs in the tissue homogenate were extracted with NucleoSpin  
19 RNA from Macherey Nagel. RNA was eluted with 50 $\mu$ L of water.

## 20 21 **Assessment of gene expression by RT-qPCR**

22 Half of the right lobe was homogenized in 1 mL of RA1 buffer from the NucleoSpin RNA kit  
23 containing 20 mM of TCEP. Total RNAs in the tissue homogenate were extracted with  
24 NucleoSpin RNA from Macherey Nagel. RNAs were eluted with 60  $\mu$ L of water.  
25 RNA was reverse-transcribed with the High-Capacity cDNA Archive Kit (Life Technologies,  
26 USA). The resulting cDNA was amplified using SYBR Green-based real-time PCR and the  
27 QuantStudio™ 12K Flex Real-Time PCR Systems (Applied Biosystems™, USA) following  
28 manufacturers protocol. Relative quantification was performed using the gene  
29 coding glyceraldehyde 3-phosphate dehydrogenase (*Gapdh*). Specific primers were designed  
30 using Primer Express software (Applied Biosystems, Villebon-sur-Yvette, France) and ordered to  
31 Eurofins Scientifics (Ebersberg, Germany). The list of primers is available in Supplementary  
32 Table 3. Relative mRNA levels ( $2^{-\Delta\Delta Ct}$ ) were determined by comparing (a) the PCR cycle  
33 thresholds (Ct) for the gene of interest and the house keeping gene ( $\Delta Ct$ ) and (b)  $\Delta Ct$  values for  
34 treated and control groups ( $\Delta\Delta Ct$ ). Data were normalized against expression of the *gapdh* gene  
35 and are expressed as a fold-increase over the mean gene expression level in mock-treated  
36 mice. Viral load is expressed as viral RNA normalized to *Gapdh* expression level ( $\Delta Ct$ ).

1  
2  
3  
4  
5  
6  
7  
8  
9  
10  
11  
12  
13  
14  
15  
16  
17  
18  
19  
20  
21  
22  
23  
24  
25  
26  
27  
28  
29  
30  
31  
32  
33  
34  
35  
36

## **Histopathology and immunohistochemical, immunofluorescence staining**

Lung tissues were fixed in 4% PBS buffered formaldehyde for 7 days, rinsed in PBS, transferred in ethanol and then processed into paraffin-embedded tissues blocks. The subcontractor Sciempath Labo (Larçay, France) performed histological processing and analysis. The tissue sections in 3 µm were stained with haematoxylin and eosin (H&E) and whole mount tissues were scanned with a Nanozoomer (Hamatsu) and the morphological changes were assessed by a semi-quantitative score. For the scoring, a dual histopathology scoring system adapted from<sup>30,31</sup> was used to assess pulmonary changes in mice. Inflammation was scored as 0 = absent, 1 = 1-10% of lung section, 2 = 11-25% of lung section, 3 = 26-50% of lung section, and 4=>50% of lung section affected.

## **Statistical analysis**

Results are expressed as the mean ± standard deviation (SD) unless otherwise stated. All statistical analysis was performed using GraphPad Prism v6 software. A Mann-Whitney *U* test was used to compare two groups unless otherwise stated. Comparisons of more than two groups with each other were analyzed with the One-way ANOVA Kruskal-Wallis test (nonparametric), followed by the Dunn's posttest. \*, P<0.05; \*\*, P<0.01; \*\*\*, P<0.001.

## **Ethics and biosafety statement**

All experiments involving SARS-CoV-2 were performed within the biosafety level 3 facility of the Institut Pasteur de Lille, after validation of the protocols by the local committee for the evaluation of the biological risks and complied with current national and institutional regulations and ethical guidelines (Institut Pasteur de Lille/B59-350009). The experimental protocols using animals were approved by the institutional ethical committee "Comité d'Ethique en Experimentation Animale (CEEA) 75, Nord Pas-de-Calais". The animal study was authorized by the "Education, Research and Innovation Ministry" under registration number APAFIS#25517-2020052608325772v3.

## **Data availability**

The data that support the findings of this study are included in the paper and Supplementary Information. Details on the composition of Apteeus drug library (TEELibrary®) are available upon request. The complete sequence of SARS-CoV-2 BetaCoV/France/IDF0372/2020 is available on GISAID EpiCoV platform (accession numbers EPI\_ISL\_406596), whereas the complete sequence of SARS-CoV-2 hCoV-19\_IPL\_France strains is available through GenBank (accession numbers and MW575140) and GISAID (accession number EPI\_ISL\_940555).

## 1 **Acknowledgements**

2 We thank Sylvie van der Werf for sharing the SARS-CoV-2 strain  
3 BetaCoV/France/IDF0372/2020, Volker Thiel for providing HCoV-229E-RLuc and Chiesi for  
4 sharing clofoctol compound. We thank the infrastructure ChemBioFrance and the platforms  
5 ARIADNE-criblage (UMS2014-US41 PLBS) and ARIADNE-ADME to provide access to the  
6 Opera microscope and for LC-MS/MS analysis. Thank are also due to Nathan François for  
7 technical assistance and to Imène Belhaouane, Robin Prath and Nicolas Vandenabele for their  
8 technical help in the BSL3 facility. We are also grateful to Françoise Jacob-Dubuisson for her  
9 helpful comment on the manuscript. The immunofluorescence analyses were performed with the  
10 help of the imaging core facility of the Bioluminescence Center Lille Nord-de-France.

11 This work was supported by the Institut Pasteur de Lille, the Fondation pour la Recherche  
12 Médicale (FRM) and the Agence Nationale de la Recherche (ANR) (Project FRM\_ANR Flash 20  
13 ANTICOV), the Centre National de la Recherche Scientifique (CNRS; COVID program) and the  
14 I-Site Foundation (I-Site\_Covid20\_ANTI-SARS2). The platform used in this work was supported  
15 by the European Union (ERC-STG INTRACELLTB grant 260901), the ANR (ANR-10-EQPX-04-  
16 01), the “Fonds Européen de Développement Régional” (Feder) (12001407 [D-AL] EquipEx  
17 ImagInEx BioMed), CPER-CTRL (Centre Transdisciplinaire de Recherche sur la Longévité) and  
18 the Région Nord-Pas-de-Calais (convention 12000080).

## 20 **Author contributions**

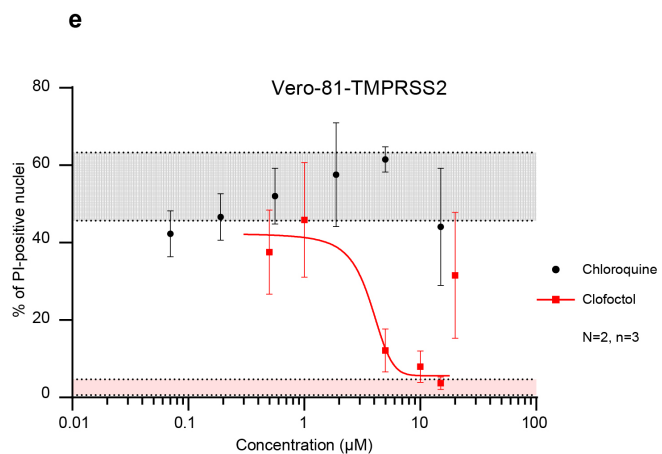
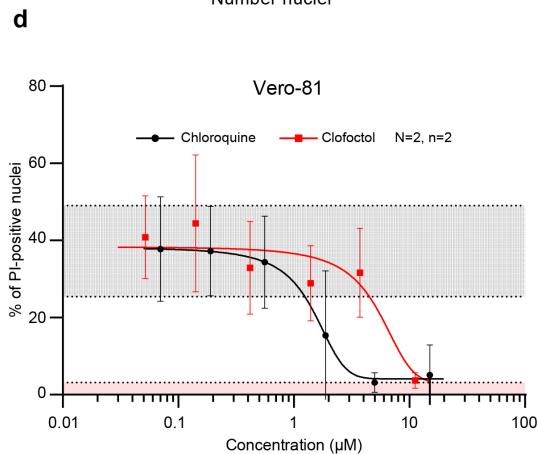
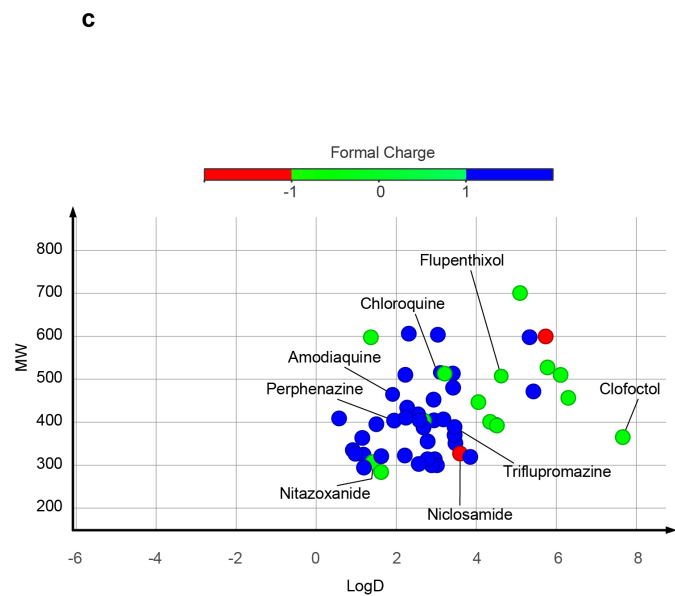
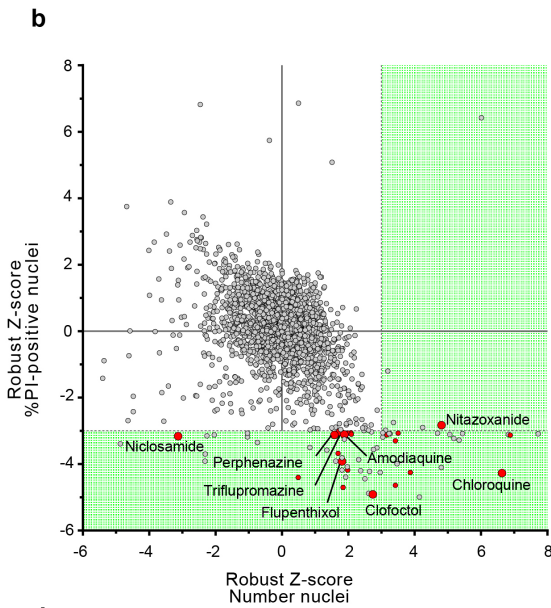
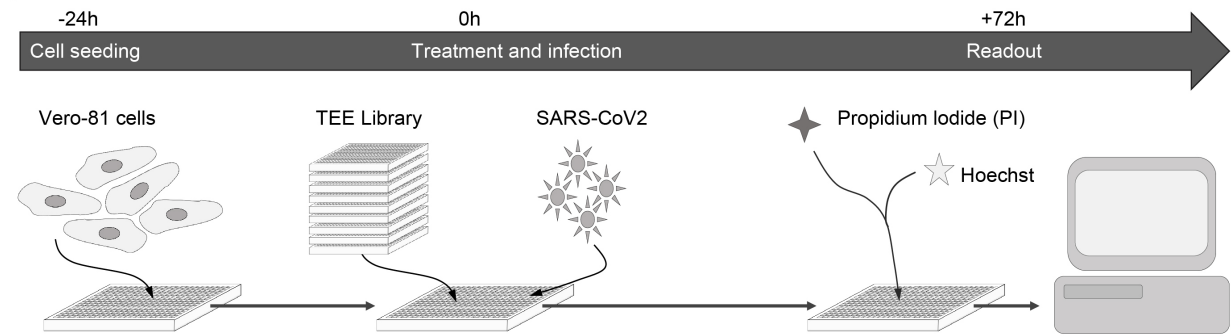
21 S.B., A.M., V.S., T.V., E.H., N.D., Y.R., Lo.D., A.D., C.R., K.S., L.B., C.M., C.P., A.B., A.V.,  
22 Lu.D., Ju. D. and F.L. designed and/or performed experiments. S.B., A.M., V.S., T.V., E.H., N.D.,  
23 Y.R., Lo.D., K.S., L.B., C.M., A.V., T.B. and S.H. analyzed data. I.E., E.K.A. and D.H. generated  
24 critical reagents. P.B., T.B., F.T., B.D. and Je.D. oversaw the conception and design of the  
25 experiments. S.B., T.V., T.B., F.T., and Je.D. wrote the manuscript.

## 27 **Competing interests**

28 T.B., L.B., C.M., S.B., P.B., N.D., B.D., Je.D., E.H., A.M., Y.R., T.V. are inventors on a patent  
29 application on repurposed antiviral activity of clofoctol against SARS-CoV-2 owned by Univ Lille,  
30 CNRS, INSERM, CHU Lille and Institut Pasteur de Lille. European Patent Application Serial No.  
31 EP20305633.8, entitled “Compound and method for the treatment of coronaviruses” relates to  
32 this work and was filed on 10 June 2020. The other authors declare no other competing  
33 interests. The corresponding authors had full access to all the data in the study and had final  
34 responsibility for the decision to submit for publication.



# 1 Figures



2  
3 **Figure 1: HCS screen of Apteous TEElibrary® for the identification of anti-SARS-CoV-2**  
4 **compounds.** a, Workflow overview of the screening process. b, Dot-plot representations of all  
5 compounds tested based on their Robust-Z-score for both the numbers of nuclei and the percentages  
6 of PI-positive nuclei. Dotted-lines are indicative of the thresholds chosen for hit selection (within the  
7 green area). c, Dot-plot representation according to the molecular weight and the LogD of the  
8 compounds of interests. Dots are color-coded based on the ionization state at physiological pH. d and  
9 e, Antiviral effect of clofoctol and chloroquine against SARS-CoV-2 on Vero-81 and Vero-81-  
10 TMRPSS2 cells. Vero-81 cells (d) and Vero-81 cells transduced with a lentiviral vector for TMPRSS2  
11 expression (e) were infected at a MOI of 0.01 in the presence of increasing concentrations of clofoctol  
12 or CQ. 72h later cells were labeled with 1 $\mu\text{g}/\text{mL}$  of propidium iodide. Pink and grey areas represent  
13 values for the infected and non-infected controls, respectively.

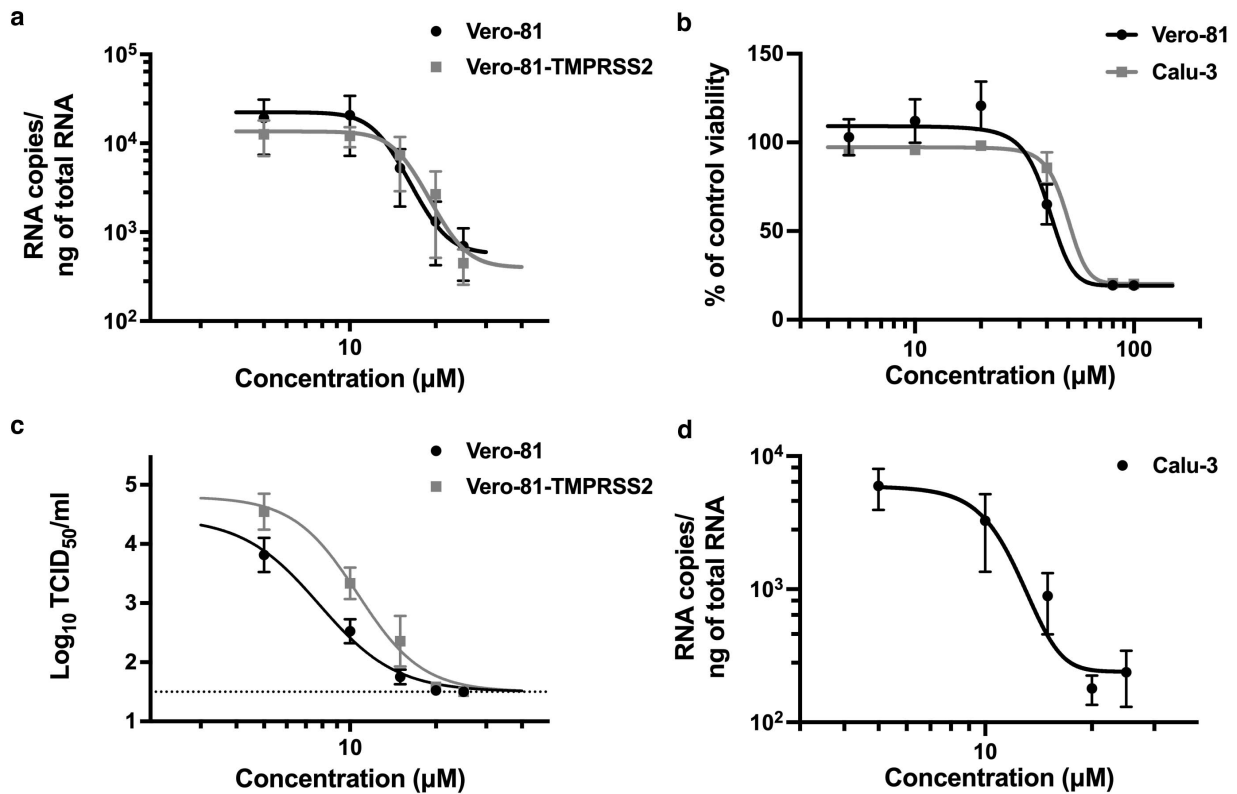
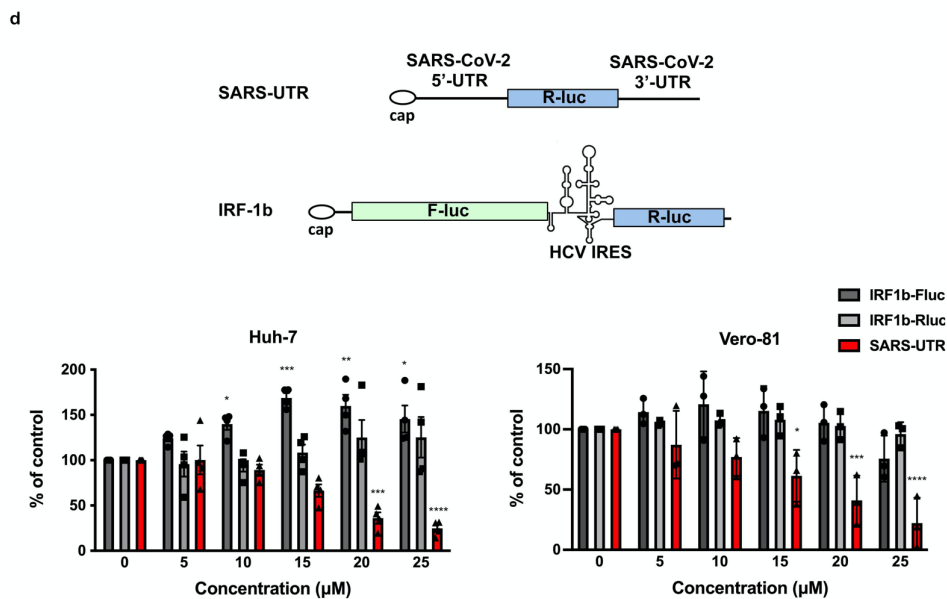
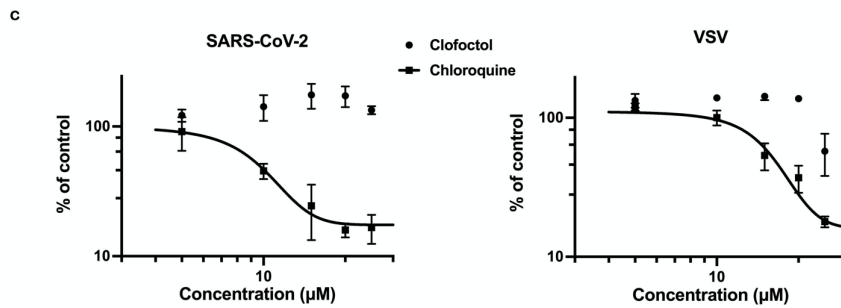
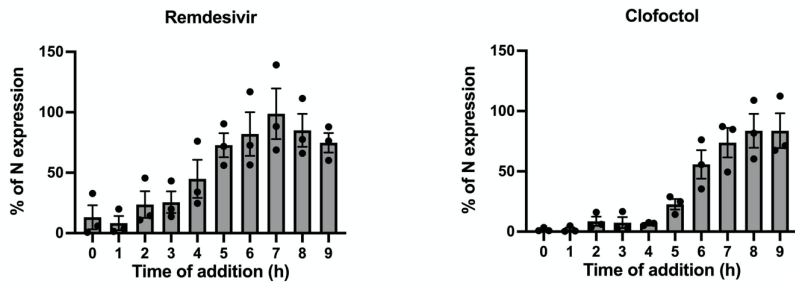
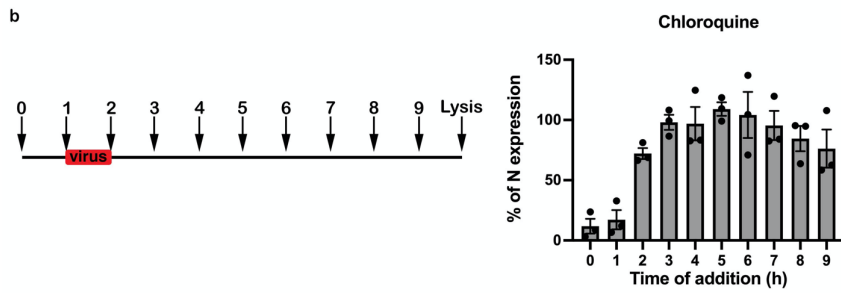
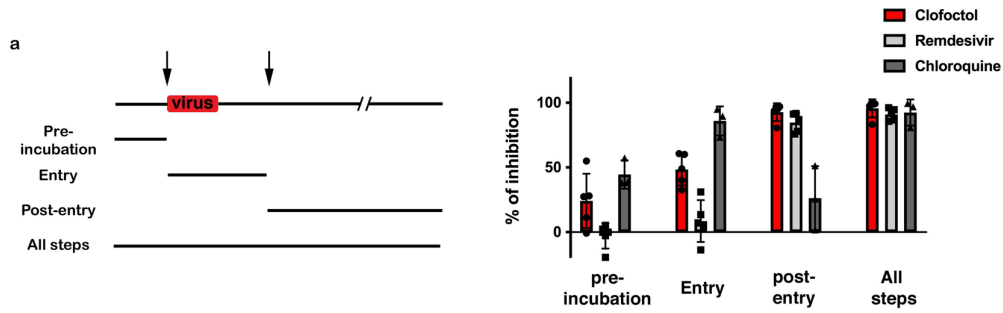
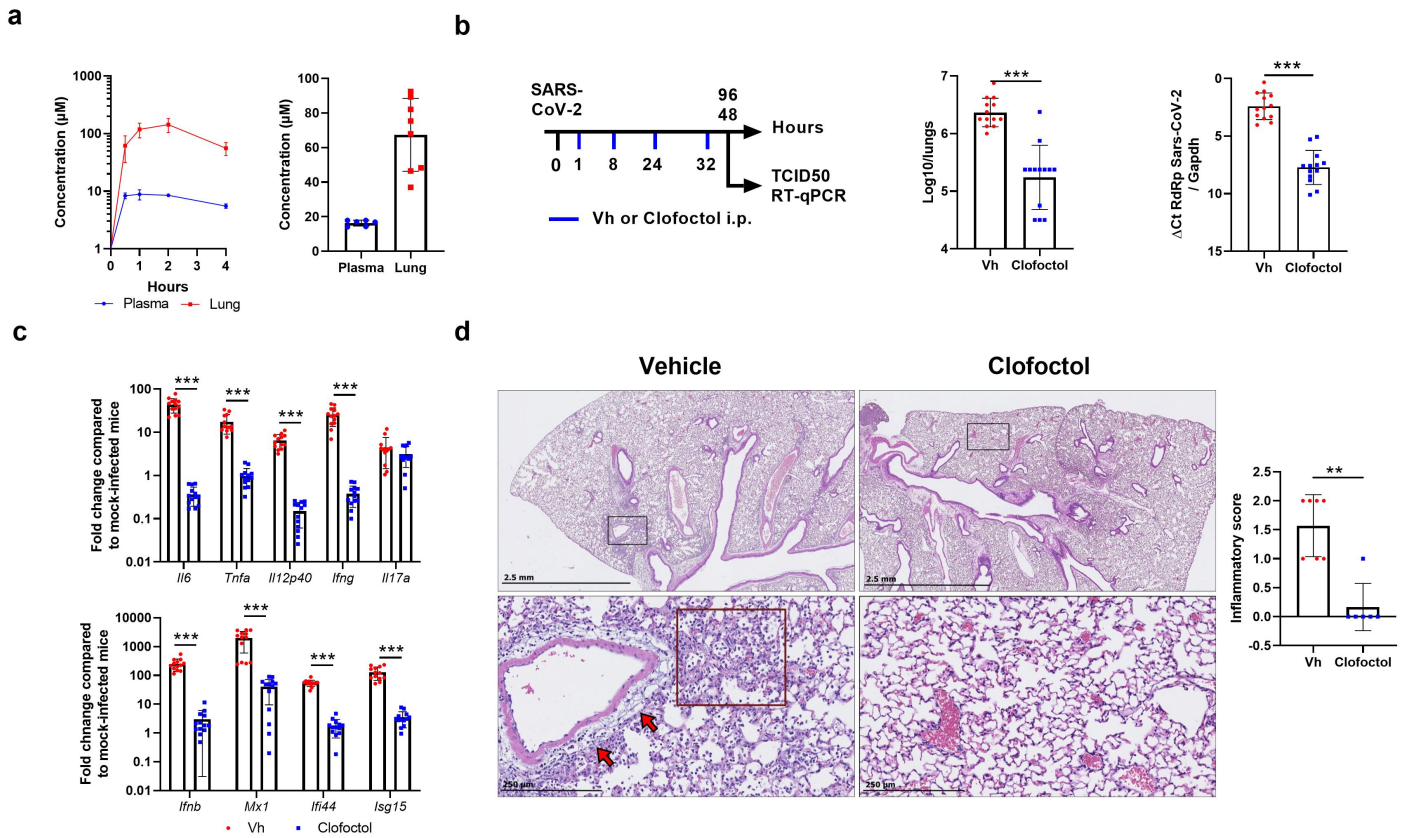


**Figure 2: In vitro validation of the antiviral activity of clofoctol.** **a**, Clofoctol inhibits the genomic replication of SARS-CoV-2. Vero-81 and Vero-81-TMPRSS2 cells were infected for 6h at a MOI of 0.25 in the presence of increasing concentrations of clofoctol. Then, total RNA was extracted and viral RNA was quantified by RT-qPCR. Results are normalized by the amount of total RNA and represent the average of three independent experiments performed in duplicates. Error bars represent the standard error of the mean (SEM). **b**, Clofoctol is not cytotoxic in cell culture at concentrations below 40 µM. Vero-81 cells and Calu-3 cells were cultured in the presence of given concentrations of clofoctol. Cell viability was monitored using the MTS-based viability assay after 24 hours of incubation. **c**, Clofoctol inhibits the production of progeny virions. Vero-81 and Vero-81-TMPRSS2 cells were infected with SARS-CoV-2 at a MOI of 0.25. After 1h, the inoculum was removed and the cells were washed with PBS prior treatment with clofoctol. Cells were then further incubated for 16h. Thereafter, supernatants were collected and the amounts of secreted infectious virus were quantified. The dotted-line represents the limit of detection (1.5 TCID<sub>50</sub>/mL). These data represent the average of three independent experiments (N=3). Experiments were performed in duplicate for each condition. **d**, Clofoctol inhibits SARS-CoV-2 replication in Calu-3 cells. Calu-3 cells were infected at a MOI of 0.25 in the presence of increasing concentrations of clofoctol for 24h. Then, total cellular RNA was extracted and viral RNA was quantified by RT-qPCR.



1  
2 Figure 3: Clofoctol targets the translation step of SARS-CoV-2 life cycle. a, Clofoctol is mainly  
3 efficient at a post-entry step. Vero-81 cells were infected with SARS-CoV-2 at a MOI of 0.25.  
4 Clofoctol, remdesivir or CQ were added at a concentration of 15  $\mu$ M either before infection,  
5 during virus entry, post-inoculation or throughout the steps as indicated. At 16h post-infection,  
6 cells were fixed with 4% paraformaldehyde and immunostained to allow for the detection of the  
7 viral double-stranded RNA. Nuclei were detected by Hoechst staining. The numbers of infected  
8 cells are expressed as a percentage of the total cell number. Results are presented as the  
9 percentage of inhibition. b, Time-of-addition experiment. Vero-81 cells were infected at a MOI of  
10 0.5 for 1h. Fifteen micromolar of clofoctol, remdesivir or CQ were added every hour starting 1h  
11 before inoculation. Cells were lysed 8h after the end of the inoculation in Laemmli loading buffer  
12 and the amount of N protein was detected in immunoblot. Results are presented as the  
13 percentage of N protein expression relative to that in non-treated cells (CTL). c, Clofoctol does  
14 not inhibit SARS-CoV-2 entry. Huh-7 cells expressing ACE2 cells were infected with SARS2pp  
15 or pseudoparticles containing the envelope glycoprotein of the vesicular stomatitis virus (VSV)  
16 used as a control (VSVpp) for 3 hours in the presence of increasing concentrations of clofoctol  
17 or CQ. At 48 hours post-infection, cells were lysed to quantify luciferase activity. The results are  
18 expressed in % of the controls of three independent experiments. The experiments were  
19 performed in triplicate (n=3) (in each condition). d, Clofoctol inhibits viral RNA translation.  
20 Schematic representation of the reporter construct expressing the *Renilla* luciferase placed  
21 between the 5'-UTR and the 3'-UTR of the SARS-CoV-2 genomic RNA and the control  
22 bicistronic construct containing the firefly luciferase sequence under the control of a cap  
23 structure, followed by the *Renilla* luciferase under the control of hepatitis C virus (HCV) IRES.  
24 Huh-7 or Vero-81 cells were electroporated with *in vitro* transcribed RNA. Cells were lysed after  
25 8h and luciferase activities were recorded. The results are expressed in % of the controls of  
26 three independent experiments. The experiments were performed in quadruplicate (n=4)(in each  
27 condition). Two-way ANOVA followed by the Dunnett's multiple comparisons test was performed  
28 for statistical analysis (\*p < 0.05; \*\*p < 0.01; \*\*\*p < 0.001).  
29  
30  
31



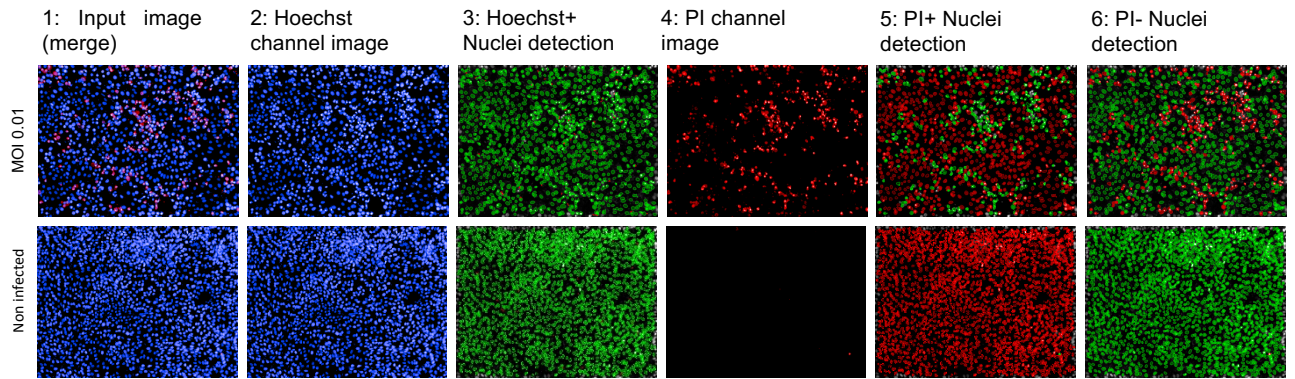
2  
 3 **Figure 4: Pharmacokinetics and antiviral properties of clofoctol in a mouse model of**  
 4 **COVID-19.** **a**, Pharmacokinetics characterization of clofoctol in mice. *Left panel*, 8-10 week-old  
 5 female C57BL/6J mice were treated i.p. with a single dose of clofoctol (62.5mg/kg) and were  
 6 sacrificed at different time points thereafter. *Right panel*, Clofoctol was inoculated twice daily  
 7 during two days and mice were sacrificed 1h after the last injection. Clofoctol concentrations in  
 8 lungs (n=3/time point, 3 samples/lung) and plasma (n=3/time point, 2 technical replicates)  
 9 are depicted. **b-d**, Effects of clofoctol treatment on SARS-CoV-2 infection in K18-hACE2 transgenic  
 10 C57BL/6J mice. **b**, *Left panel*, Scheme of the experimental design in which the effects of  
 11 clofoctol was assessed in mice. Mice were treated i.p. with clofoctol (62.5mg/kg) or vehicle 1h  
 12 and 8h after i.n. inoculation of SARS-CoV-2 ( $5 \times 10^2$  TCID<sub>50</sub> per mouse) and treated again twice  
 13 at day 1 post-infection. Animals were sacrificed at day 2 and day 4 post-infection. The viral load  
 14 was determined by titration on Vero-E6 cells (*middle panel*) and by RT-qPCR (*right panel*) (day 2  
 15 post-infection). **c**, mRNA copy numbers of genes were quantified by RT-qPCR. Data are  
 16 expressed as fold change over average gene expression in mock-treated (uninfected) animals  
 17 (day 2 post-infection). **d**, Lung sections were analyzed at day 4 post-infection. Shown are  
 18 representative lungs (hematoxylin and eosin staining). *Lower panels*, enlarged views of the area  
 19 circled in black in *upper panels*. Blinded sections were scored for levels of pathological severity.  
 20 The inflammatory score is depicted. **b-c**, Results are expressed as the mean  $\pm$  SD (n=13 for  
 21 panels **b** and **c** and n=6-7 for panel **d**). Significant differences were determined using the Mann-  
 22 Whitney U test (\*\*p < 0.01; \*\*\*p < 0.001).

1 **Supplementary Table S1**

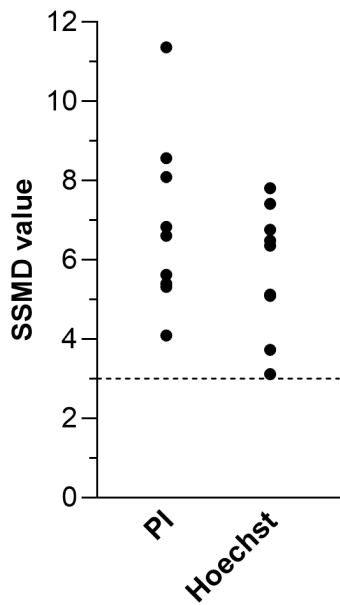
2 **Multi-parametric script used in Columbus (version 2.3.1, PerkinElmer) for the determination of the**  
 3 **percentage of PI+ Nuclei (PI-positive nuclei related to Fig. 1b).**

<b>Input Image</b>	<b>Stack Processing:</b> Individual Planes <b>Flat field Correction:</b> None	<b>Method</b>	<b>Output</b>
<b>Calculate Image</b>		<b>Method</b> : By Formula Formula : iif(A>100,A,0) Channel A : Exp1Cam1 Negative Values : Set to Zero Undefined Values : Set to Local Average	Output Image : Hoechst Mask
<b>Find Nuclei</b>	Channel : Hoechst Mask ROI : None	Method : C Common Threshold : <u>0.1</u> Area : > 5 $\mu\text{m}^2$ Splitting Coefficient : 9 Individual Threshold : 0 Contrast : > -1	Output Population : Nuclei
<b>Select Population</b>	Population : Nuclei	Method : Common Filters Remove Border Objects Region : Nucleus	Output Population : Hoechst+ Nuclei preSelected
<b>Calculate Morphology Properties</b>	Population : Hoechst+ Nuclei preSelected Region : Nucleus	Method : Standard Area Roundness	Output Properties : Hoechst+ Nuclei preSelected
<b>Select Population</b>	Population : Hoechst+ Nuclei preSelected	Method : Filter by Property Hoechst+ Nuclei preSelected Area [px <sup>2</sup> ] : >= 35 Hoechst+ Nuclei preSelected Roundness : >= <u>0.5</u> Boolean Operations : F1 and F2	Output Population : <b>Hoechst+ Nuclei</b>
<b>Calculate Intensity Properties</b>	Channel : Exp1Cam2 Population : <b>Hoechst+ Nuclei</b> Region : Nucleus	<b>Method</b> : Standard Mean	Output Image : PI Intensity Nucleus
<b>Select Population</b>	Population : <b>Hoechst+ Nuclei</b>	Method : Filter by Property PI Intensity Nucleus Mean : 65	Output Population : <b>PI+ Nuclei</b>
<b>Select Population</b>	Population : <b>Hoechst+ Nuclei</b>	Method : Filter by Property PI Intensity Nucleus Mean : 65	Output Population : <b>PI- Nuclei</b>
<b>Define Results</b>	Method : List of Outputs Population : <b>Hoechst+ Nuclei</b> Number of Objects Population : <b>PI+ Nuclei</b> Number of Objects Population : <b>PI- Nuclei</b> Number of Objects Method : Formula Output Formula : a/b*100 Population Type : Objects Variable A : <b>PI+ Nuclei</b> - Number of Objects Variable B : <b>Hoechst+ Nuclei</b> - Number of Objects Output Name : <b>% PI+ Nuclei</b>		

1  
2  
3  
4  
5  
6  
7  
8  
9  
10  
11  
12  
13  
14  
15

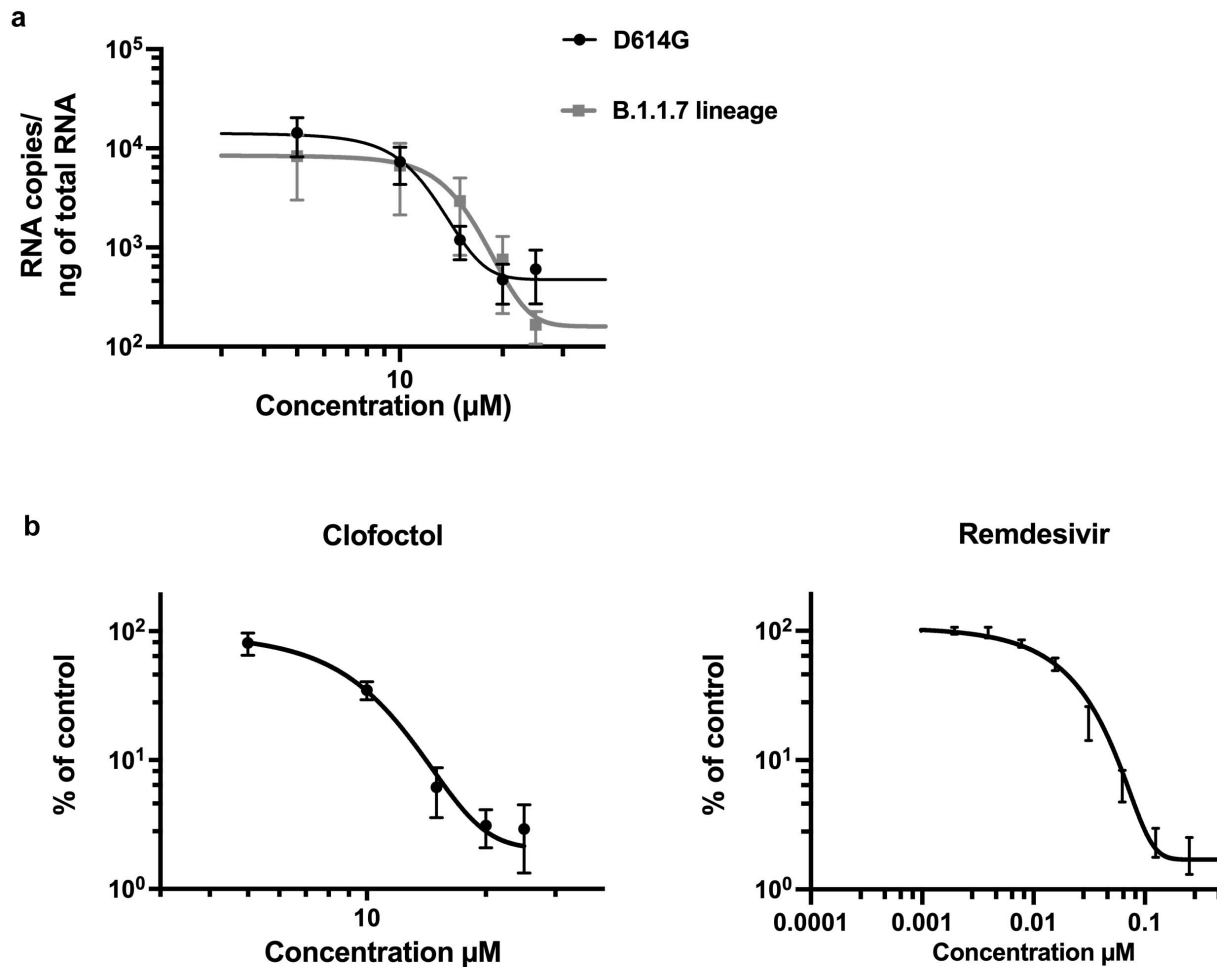


b



16  
17  
18  
19  
20  
21  
22  
23  
24  
25  
26  
27  
28  
29  
30  
31  
32  
33  
34  
35  
36

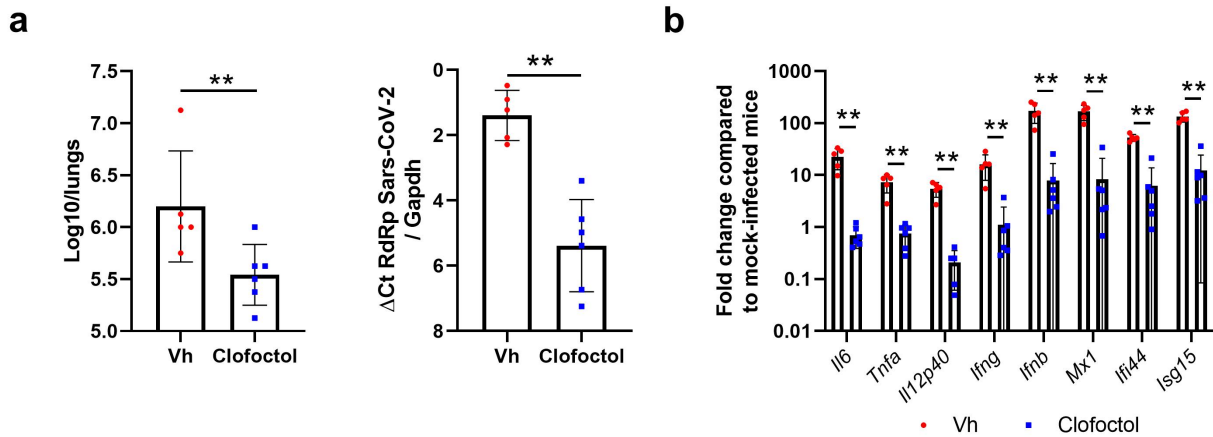
**Figure S1: a**, Typical images of Vero-81 cells infected with SARS-Cov-2 (top panel: MOI=0.01) or not (lower panel: Non-infected) acquired on an OPERA™ High Content Screening System (PerkinElmer) and corresponding image segmentation. 1: Typical 2-color images (Blue: Hoechst label, Red: PI-label); 2 and 4: 1-color images corresponding respectively to Hoechst and PI channel images; 3: Filled green objects correspond to total segmented nuclei, 5: Filled green objects correspond to PI positive cells or dead segmented cells, 6: Circled green cells correspond to non-infected cells. **b** SSMD values for HCS screen of the Apteus TEELibrary® for the identification of anti-SARS-CoV-2 compounds. SSMD values were calculated for each of the 9 plates by comparing mean and standard deviations on both negative (Mock) and positive (Infected) controls. Dotted-line is indicative of a threshold of 3 allowing for the validation of the plates. SSMDs were calculated for both readouts.



1  
2 **Figure S2: Clofoctol inhibits other SARS-CoV-2 variants as well as HCoV-229E.** a, Vero-81  
3 cells were infected either with SARS-CoV-2 of lineage B1 containing the D614G mutation  
4 (SARS-CoV-2/human/FRA/Lille\_Vero-TMPRSS2/2020) or with SARS-CoV-2 of lineage B.1.1.7  
5 (GISAID accession number EPI\_ISL\_1653931). Viral genomes were quantified by RT-qPCR.  
6 Results are normalized by the amount of total RNA and represent the average of three  
7 independent experiments performed in duplicates. **b**, Huh-7 cells were infected with HCoV-  
8 229E-Rluc in presence of different concentrations of clofoctol or remdesivir. At 7h post-infection,  
9 cells were lysed and luciferase activities were quantified. Results are presented as the  
10 percentages of the control and represent an average of three independent experiments  
11 performed in triplicates. Errors bars represent the standard error of the mean (SEM).  
12



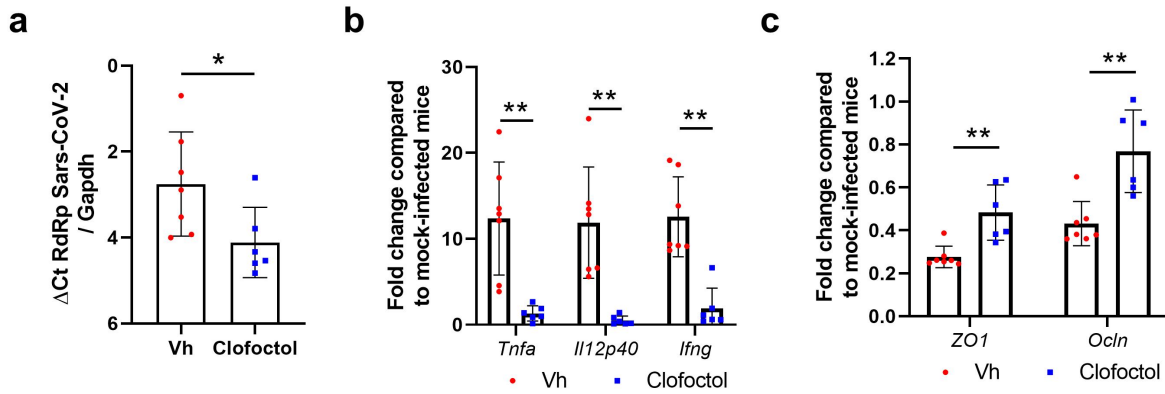
1  
2



3  
4  
5  
6  
7  
8  
9  
10  
11  
12

**Figure S3: Effects of clofocetol treatment in male K18-hACE2 transgenic mice. a and b,** Male mice were treated (50 mg/kg of clofocetol) and infected as described in Figure 4b. Mice were sacrificed at day 2 post-infection. **a**, The viral load was determined by titration on Vero-E6 cells (*left panel*) and by RT-qPCR (*right panel*). **b**, mRNA copy numbers of genes were quantified by RT-qPCR. Data are expressed as fold change over average gene expression in mock-treated (uninfected) animals. Results are expressed as the mean ± SD (n=5-6). Significant differences were determined using the Mann-Whitney U test (\*\*p < 0.01).

1  
2



## 1 References

- 2 1. Arthi, V. & Parman, J. Disease, downturns, and wellbeing: Economic history and the long-  
3 run impacts of COVID-19. *Explor. Econ. Hist.* **79**, 101381 (2021).
- 4 2. WHO Solidarity Trial Consortium *et al.* Repurposed Antiviral Drugs for Covid-19 - Interim  
5 WHO Solidarity Trial Results. *N. Engl. J. Med.* **384**, 497–511 (2021).
- 6 3. Jeon, S. *et al.* Identification of Antiviral Drug Candidates against SARS-CoV-2 from FDA-  
7 Approved Drugs. *Antimicrob. Agents Chemother.* **64**, (2020).
- 8 4. Riva, L. *et al.* Discovery of SARS-CoV-2 antiviral drugs through large-scale compound  
9 repurposing. *Nature* **586**, 113–119 (2020).
- 10 5. Yuan, S. *et al.* Clofazimine broadly inhibits coronaviruses including SARS-CoV-2. *Nature*  
11 (2021) doi:10.1038/s41586-021-03431-4.
- 12 6. Matsuyama, S. *et al.* Enhanced isolation of SARS-CoV-2 by TMPRSS2-expressing cells.  
13 *Proc. Natl. Acad. Sci. U. S. A.* **117**, 7001–7003 (2020).
- 14 7. Wang, M. *et al.* Remdesivir and chloroquine effectively inhibit the recently emerged novel  
15 coronavirus (2019-nCoV) in vitro. *Cell Res.* **30**, 269–271 (2020).
- 16 8. Lu, J. *et al.* Screened antipsychotic drugs inhibit SARS-CoV-2 binding with ACE2 in vitro.  
17 *Life Sci.* **266**, 118889 (2021).
- 18 9. Weston, S. *et al.* Broad Anti-coronavirus Activity of Food and Drug Administration-Approved  
19 Drugs against SARS-CoV-2 In Vitro and SARS-CoV In Vivo. *J. Virol.* **94**, (2020).
- 20 10. Hoffmann, M. *et al.* Chloroquine does not inhibit infection of human lung cells with SARS-  
21 CoV-2. *Nature* (2020) doi:10.1038/s41586-020-2575-3.
- 22 11. Del Tacca, M. *et al.* Penetration of clofocetol into human lung. *J. Antimicrob. Chemother.* **19**,  
23 679–683 (1987).
- 24 12. Lo, M. K. *et al.* Remdesivir targets a structurally analogous region of the Ebola virus and  
25 SARS-CoV-2 polymerases. *Proc. Natl. Acad. Sci. U. S. A.* **117**, 26946–26954 (2020).
- 26 13. Goueslain, L. *et al.* Identification of GBF1 as a cellular factor required for hepatitis C virus  
27 RNA replication. *J. Virol.* **84**, 773–787 (2010).
- 28 14. Golden, J. W. *et al.* Human angiotensin-converting enzyme 2 transgenic mice infected with  
29 SARS-CoV-2 develop severe and fatal respiratory disease. *JCI Insight* **5**(19):e142032 (2020).
- 30 15. Danesi, R. & Del Tacca, M. Clinical study on the efficacy of clofocetol in the treatment of  
31 infectious respiratory diseases. *Int. J. Clin. Pharmacol. Res.* **5**, 175–179 (1985).
- 32 16. Ghilardi, P. L. & Casani, A. Treatment of ear, nose and throat infections with clofocetol. *Drugs*  
33 *Exp. Clin. Res.* **11**, 815–818 (1985).
- 34 17. Yablonsky, F. Alteration of membrane permeability in *Bacillus subtilis* by clofocetol. *J. Gen.*  
35 *Microbiol.* **129**, 1089–1095 (1983).
- 36 18. Yablonsky, F. & Simonnet, G. Action of clofocetol on bacterial cell wall synthesis. *J.*  
37 *Pharmacol.* **13**, 515–524 (1982).
- 38 19. Hu, Y. *et al.* The antibiotic clofocetol suppresses glioma stem cell proliferation by activating  
39 KLF13. *J. Clin. Invest.* **129**, 3072–3085 (2019).
- 40 20. Wang, M. *et al.* Identification of an old antibiotic clofocetol as a novel activator of unfolded  
41 protein response pathways and an inhibitor of prostate cancer. *Br. J. Pharmacol.* **171**, 4478–  
42 4489 (2014).
- 43 21. Bailly, C. & Vergoten, G. A new horizon for the old antibacterial drug clofocetol. *Drug Discov.*  
44 *Today* (2021) doi:10.1016/j.drudis.2021.02.004.
- 45 22. Wang, Y. *et al.* Triggering unfolded protein response by 2-Deoxy-D-glucose inhibits porcine  
46 epidemic diarrhea virus propagation. *Antiviral Res.* **106**, 33–41 (2014).
- 47 23. Xue, M. *et al.* The PERK Arm of the Unfolded Protein Response Negatively Regulates

- 1 Transmissible Gastroenteritis Virus Replication by Suppressing Protein Translation and  
2 Promoting Type I Interferon Production. *J. Virol.* **92**, (2018).
- 3 24. Alessandri, M. G. *et al.* The pharmacokinetic profile of clofoctol in rat plasma and tissues  
4 after oral and rectal administration. *Drugs Exp. Clin. Res.* **12**, 343–347 (1986).
- 5 25. Fernandez-Zapico, M. E. *et al.* A functional family-wide screening of SP/KLF proteins  
6 identifies a subset of suppressors of KRAS-mediated cell growth. *Biochem. J.* **435**, 529–537  
7 (2011).
- 8 26. Jiang, S. *et al.* KLF13 promotes porcine adipocyte differentiation through PPAR $\gamma$  activation.  
9 *Cell Biosci.* **5**, 28 (2015).
- 10 27. Nakabayashi, H., Taketa, K., Miyano, K., Yamane, T. & Sato, J. Growth of human hepatoma  
11 cells lines with differentiated functions in chemically defined medium. *Cancer Res.* **42**, 3858–  
12 3863 (1982).
- 13 28. Song, O.-R. *et al.* Phenotypic assays for Mycobacterium tuberculosis infection. *Cytom. Part*  
14 *J. Int. Soc. Anal. Cytol.* **91**, 983–994 (2017).
- 15 29. Eymieux, S. *et al.* Ultrastructural modifications induced by SARS-CoV-2 in Vero cells: a  
16 kinetic analysis of viral factory formation, viral particle morphogenesis and virion release. *Cell.*  
17 *Mol. Life Sci.* (2021) doi:10.1007/s00018-020-03745-y.
- 18 30. Imai, M. *et al.* Syrian hamsters as a small animal model for SARS-CoV-2 infection and  
19 countermeasure development. *Proc. Natl. Acad. Sci. U. S. A.* **117**, 16587–16595 (2020).
- 20 31. Meyerholz, D. K. & Beck, A. P. Histopathologic Evaluation and Scoring of Viral Lung  
21 Infection. *Methods Mol. Biol. Clifton NJ* **2099**, 205–220 (2020).
- 22